The effect of surge on riverine flood hazard and impact in deltas globally

Authors and addresses

Dirk Eilander[1,2], Anaïs Couasnon[1], Hiroaki Ikeuchi[3], Sanne Muis[1,2], Dai Yamazaki[4], Hessel C. Winsemius[2,5], Philip J. Ward[1]

1. Institute for Environmental Studies (IVM), Vrije Universiteit Amsterdam, Amsterdam, Netherlands
2. Deltares, Delft, The Netherlands
3. Ministry of Land, Infrastructure, Transport and Tourism, Kyoto, Japan
4. Institute of Industrial Sciences, the University of Tokyo, Tokyo, Japan
5. Delft University of Technology, Delft, the Netherlands

Keywords

Compound flooding; Flood modelling; Model coupling; Flood hazard; Flood impact

Abstract

Current global riverine flood risk studies assume a constant mean sea level boundary. In reality high sea levels can propagate up a river, impede high river discharge, thus leading to elevated water levels. Riverine flood risk in deltas may therefore be underestimated. This paper presents the first global scale assessment of the joint influence of riverine and coastal drivers of flooding in deltas. We show that if storm surge is ignored, flood depths are significantly underestimated for 9.3% of the expected annual population exposed to riverine flooding. The assessment is based on extreme water levels at 3433 river mouth locations as modeled by a state-of-the-art global river routing model, forced with a multi-model runoff ensemble and bounded by dynamic sea level conditions derived from a global tide and surge reanalysis. We first classified the drivers of riverine flooding at each location into four classes: surge-dominant, discharge-dominant, compound-dominant or insignificant. We then developed a model experiment to quantify the effect of surge on flood hazard and impacts. Drivers of riverine flooding are compound-dominant at 19.7% of the locations analyzed, discharge-dominant at 69.2%, and surge-dominant at 7.8%. Compared to locations with either surge- or discharge-dominant flood drivers, locations with compound-dominant flood drivers generally have larger surge extremes and are located in basins with faster discharge response and/or flat topography. Globally, surge exacerbates 1-in-10 years flood levels at 64.0% of the locations analyzed, with a mean increase of 11 cm. While this increase is generally larger at locations with compound- or surge-dominant flood drivers, flood levels also increase at locations with discharge-dominant flood drivers. This study underlines the importance of including dynamic downstream sea level boundaries in (global) riverine flood risk studies.

MAIN TEXT

1 Introduction

Currently, global flood risk studies either examine riverine or coastal floods (Dottori *et al* 2018, Hallegatte *et al* 2013, Hinkel *et al* 2014, Hirabayashi *et al* 2013, Jongman *et al* 2012, Ward *et al* 2013, 2017, Vitousek *et al* 2017, Vousdoukas *et al* 2018, Winsemius *et al* 2016). As such, these studies have not accounted for compound events, in which the combination of multiple drivers and/or hazards can interact to modulate risk (Zscheischler *et al* 2018). Compound flood events can occur from the interplay between riverine and coastal flood drivers, for instance when: high sea levels propagate up a river leading to elevated water levels; and/or the drainage of high river discharge is impeded by elevated sea levels. Current riverine flood hazard models ignore these interactions and potential dependencies between riverine and coastal flood drivers, which may result in an under- or overestimation of flood risk (Wahl *et al* 2015, Ward *et al* 2018). A first step towards accounting for compound events in global flood risk assessments is to understand where, and under which conditions, compound events modulate flood hazard.

Several studies have addressed this by examining statistical dependence between different riverine and coastal flood drivers. They find dependence between: storm surge and precipitation in Australia (Wu *et al* 2017, 2018, Zheng *et al* 2013), the United States (Moftakhari *et al* 2017, Wahl *et al* 2015), Europe (Bevacqua *et al* 2019, Petroliagkis 2017), and the Netherlands (Van Den Hurk *et al* 2015, Ridder *et al* 2018); and storm surge and discharge in various parts of the United Kingdom (Hendry *et al* 2019, Lamb *et al* 2010, Svensson and Jones 2002, 2004), the Netherlands (Kew *et al* 2013, Khanal *et al* 2019, Klerk *et al* 2015), Texas (USA) (Couasnon *et al* 2018) and Italy (Bevacqua *et al* 2017). At the global scale significant dependence between storm surge and discharge based on observations was found at more than half of the locations studied (Ward *et al* 2018) and based on simulations at 26% of the locations studied (Couasnon *et al* 2019).

A limitation of these dependence-based analyses is the need for event selection based on the flood drivers (e.g. surge or discharge) rather than water levels. This introduces bias in the joint probability estimate, as events are either conditioned on one driver or on the other (Hawkes 2008, Zheng *et al* 2014). Furthermore, extreme water levels might be driven by events that are not extreme themselves (Serafin *et al* 2019). Van den Hurk *et al* (2015) were the first to carry out an impact-based analysis of compound events (i.e. based on the impact of compound flood drivers rather than their dependence) for a case study of a near-flood event in the Netherlands. An ensemble of surge and precipitation time-series were simulated with a regional climate model and used to force a hydrodynamic model of the inland water system. The simulated time-series were shuffled to remove dependence between surge and discharge. By comparing simulated water levels from original and `shuffled' time-series, the effect of surge-precipitation dependence on extreme inland water levels was examined. This approach eliminates the need for a-priori event selection but requires models that realistically simulate interactions between multiple drivers.

At the global scale, the first river routing model to account for surge-discharge interactions was presented by Ikeuchi *et al* (2017). They included dynamic downstream sea level conditions in the global river routing model CaMa-Flood (Yamazaki *et al* 2011) by coupling it to the Global Tide and Surge Model (GTSM; Muis *et al* 2016). They show a significant difference in the annual maxima of riverine water levels between simulations using dynamic sea level boundary conditions and those using static mean sea levels. However, they did not assess the drivers of extreme water levels nor the effect of surge on flood levels specifically, leaving the question unanswered as to where, and to what extent, compound surge affects flooding.

To date, no global analysis of surge-discharge interactions based on simulated water levels exists. To fill this gap, we developed a global compound flood model framework with the aim to identify dominant flood drivers in deltas globally and assess the effect of surge on riverine flood hazard and impact. This is an important step towards including compound flood events in global flood risk modelling.

2 Methods

We developed a model framework consisting of a global river routing model forced by a multi-model ensemble of global hydrological models and bounded downstream by a global tide and surge model (section 2.1). We analyzed simulated water levels from the model framework to classify the dominant driver of riverine flooding in deltas globally (section 2.2); to assess the effect of surge on flood hazard (section 2.3); and flood impact in terms of population exposed (section 2.4).

2.1 Model framework

We developed a model framework for global compound flood simulations, see Figure 1. We used a multi-model ensemble of runoff from tier 2 of the EartH2Observe (E2O) project (Dutra *et al* 2017, Schellekens *et al* 2017) with meteorological forcing from ERA-Interim (Dee *et al* 2011) and MSWEP v1.2 (Beck *et al* 2017), surge levels from the Global Tide and Surge Reanalysis (GTSR) based on the GTSM model (Muis *et al* 2016), and tide levels from the FES2012 model (Carrere *et al* 2012). These runoff and dynamic sea level (surge and tide) data were used to force the global river routing model CaMa-Flood (Yamazaki *et al* 2011) to simulate riverine water levels and flood depths. Each model component is further discussed in this section.

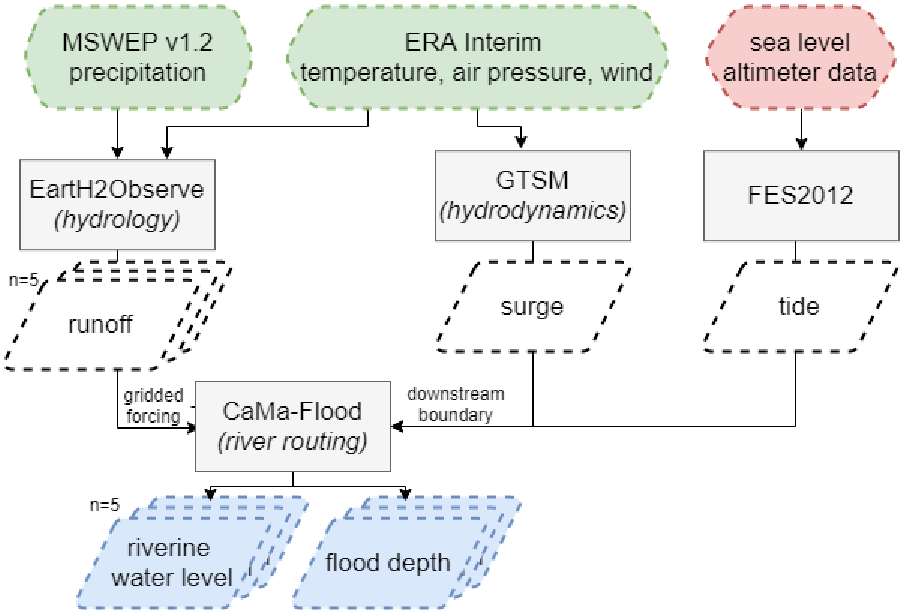

Figure 1: Model framework showing: the individual hydrologic and hydrodynamic models (grey); the meteorological forcing (green); tidal forcing (red); intermediate outputs (white); and final output used in our analysis (blue).

CaMa-Flood solves the local inertial equation (Bates *et al* 2010, Yamazaki *et al* 2013) and has a 1D routing scheme derived from HydroSHEDS (Lehner *et al* 2008) with explicit representation of floodplains. It was selected as it is the first global river routing model to include a dynamic downstream sea level boundary (Ikeuchi *et al* 2017) and has good performance for discharge extremes (Zhao *et al* 2017). CaMa-Flood and GTSM do not have a perfectly joined interface: The most downstream river point in CaMa-Flood (hereafter referred to as river mouth) is often located inside the estuary, whereas GTSM output locations are slightly offshore. We therefore assumed a simplified estuary to schematize the missing link between the CaMa-Flood river mouth and GTSM. As the exact shape and bathymetry of estuaries globally is unknown, we extrapolated the channel width and depth from the CaMa-Flood river mouth, keeping the depth constant (Savenije 2005) and with a set length of 10 km. This estuary channel length is based on extensive validation by Ikeuchi *et al* (2017). River mouths in CaMa-Flood were coupled to the nearest GTSM output location within a maximum distance of 75 km. This distance threshold was selected as a trade-off between including as many river mouths as possible and excluding unrealistic links with GTSM output locations. Due to the relatively coarse resolution of the hydrological models, we focused on catchments with a minimum catchment size of 1000 km^2. Using these criteria, a downstream boundary was set for 3433 river mouths based on 2352 GTSM output locations. We ran CaMa-flood with default settings at 15' resolution for the period 1980-2014, with a spin-up period of two years using repeated forcing from the first year.

Runoff forcing data were obtained from the state-of-the-art global multi-model ensemble of E2O tier 2 (Dutra *et al* 2017, Schellekens *et al* 2017), representing the uncertainty in land surface and hydrological processes. From the available models we selected five that assume natural conditions, i.e. without anthropogenic water extractions (Table 1). The runoff data were preprocessed to be on an identical grid with 15' resolution from 90 North to 60 South, re-defined as a positive flux, and negative runoff values were set to zero in the JULES and ORCHIDEE data after discussions with the data owners (personal communication, 2018). We validated simulated discharge from CaMa-Flood forced by the E2O runoff ensemble against observations from the Global Runoff Data Centre with a focus on the magnitude and timing of discharge extremes. Although we find a large spread between individual models, the ensemble-mean performance statistics generally shows low model bias and small time lags compared to observations (see supplementary information).

GTSM is the first global hydrodynamic model to simulate surge levels (i.e. the response of the sea surface to changes in atmospheric pressure and wind speed (Pugh and Woodworth, 2014)) with sufficiently high temporal and spatial resolution for this application (i.e. near-shore resolution of 2.5 km). It has good performance compared to tide gauge data and other models (Cid *et al* 2018, Muis *et al* 2017, Wahl *et al* 2017) and the timing and magnitude of storm surge peaks display sufficient performance for global scale compound flood analysis (Couasnon *et al* 2019). FES2012 simulates tides based on 32 tidal constituents and assimilation of satellite altimetry data (Carrere *et al* 2012) and is proven to have good near-shore performance (Stammer *et al* 2014). Mean sea level, tide, and surge are linearly superimposed to yield time-series of total still water levels at a 30-minute temporal resolution, thereby ignoring non-linear surge-tide interactions. A correction was applied to convert the vertical reference of still water levels from MSL to Earth Gravitational Model 1996 based on Mean Dynamic Topography data from Rio *et al* (2014), following Muis *et al* (2017).

Table 1: E2O WRR2 multi-model ensemble of global hydrological models (GHMs) and land surface models (LSMs); based on Schellekens *et al* (2017) and Dutra *et al* (2017).

Model	Model type	Runoff process representation	Reference
HTESSEL	LSM	Saturation excess	(*Balsamo et al.*, 2009)
JULES	LSM	Saturation and infiltration excess	(*Best et al.*, 2011; *Clark et al.*, 2011)
LISFLOOD	GHM	Saturation and infiltration excess	(*Van Der Knijff et al.*, 2010)
ORCHIDEE	LSM	Green-Ampt infiltration	(*Krinner et al.*, 2005)
W3RA	GHM	Saturation and infiltration excess	(*Van Dijk et al.*, 2014)

2.2 Flood drivers

We classified the dominant drivers of flooding at each river mouth location, represented by annual maximum riverine water levels (h_{AM}), into four classes: surge-dominant, discharge-dominant, compound-dominant or insignificant. The classification is based on the rank correlations between both h_{AM} and discharge and h_{AM} and skew surge (i.e. vertical difference between maximum still water level and high tide in a tidal cycle). We used skew surge as it is the quantity of total water levels that might lead to flooding (Haigh *et al* 2016). Discharge and skew surge are selected as the maximum value within a 1-day window of the h_{AM} event to account for delayed responses of riverine water levels and to find sub-daily skew surge peaks. Where both discharge and skew surge display a significant positive correlation (p=0.05) with h_{AM} in a majority of the ensemble members, the flood drivers are classified as compound-dominant. Where either the discharge or the surge driver displays a significant positive correlation with h_{AM} in a majority of the ensemble members, flood drivers at this location are classified as discharge- or surge-dominant respectively. Locations where neither driver displays significant correlation in a majority of the ensemble members are classified as insignificant. The classification is illustrated for three contrasting locations in Figure 2, where the drivers of flooding at the river mouths are classified as (a) surge-dominant, (b) discharge-dominant, or (c) compound-dominant. At the Mattepone River (c), large flood events (darker colors) are caused by either high skew surge or discharge or a combination of moderate skew surge and discharge. At the Dal (a) and Volta (b) rivers, large flood events are primarily caused by a single driver and extreme water levels can largely be explained using a univariate extreme value distribution. The return periods for h_{AM} do not always result in perfect contours as some drivers (such as astronomical tide and waves) are not included, but also due to non-linear interactions between surge and discharge (Serafin *et al* 2019). This illustrates the relevance of studying compound events based on water levels rather than their individual drivers.

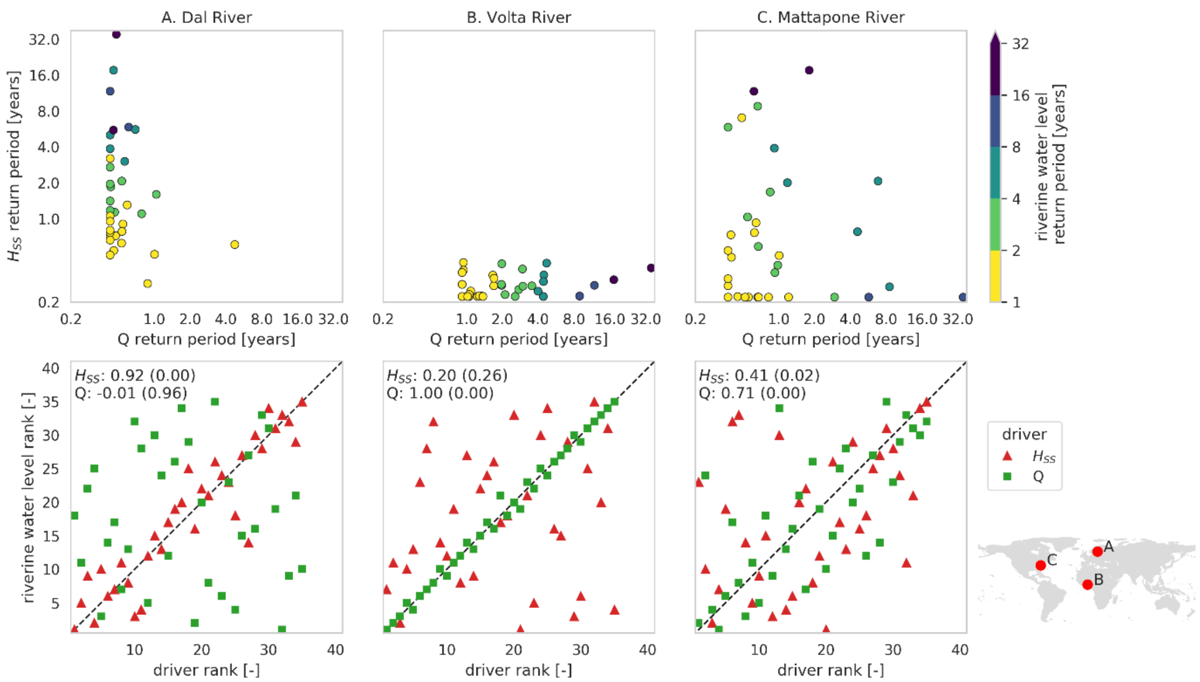

Figure 2: Classification of flood drivers illustrated for three contrasting locations based on the JULES

model, a single ensemble-member, with (**top row**) the empirical return periods based on annual maxima riverine water level events h_{AM} as function of the empirical return period of its drivers skew surge (H_{SS}, y-axis) and discharge (Q, x-axis); and (**bottom row**) the spearman rank correlation between h_{AM} events and H_{SS} (red triangles) and h_{AM} events and Q (green squares).

2.3 **Flood levels**

We developed three experiments, see Table 2, to assess the difference in extreme riverine water levels with and without surge components. Surge levels were divided into a daily and seasonal component to assess their relative effects on flood levels. The seasonal component is associated with seasonal gyre circulation driven by synoptic pressure and wind differences at time scales longer than one month (e.g. Yang *et al* 1998, Palma *et al* 2004) and computed as monthly mean surge levels. The daily component is associated with surge due to short term meteorological variations in wind speed and sea level pressure and is computed as the difference between the total variation and seasonal component. Extreme water levels are derived based on the 2-parameter Gumbel distribution fitted to annual maxima using the L-moments method (Hosking and Wallis 2005). Confidence intervals (5^{th}-95^{th} percentiles) are obtained from bootstrapping with a sample size of 1000, where the Gumbel parameters are bias-corrected for the mean of bootstrap parameter samples.

Table 2: Experiments to assess the effect of surge (components) on flood levels and impact based on the difference between the described scenarios

Experiment	Dynamic downstream sea level boundary	
	Scenario A	Scenario B
1. Total surge	Tide and total surge levels	Tide
2. Seasonal component	Tide and seasonal surge levels	Tide
3. Daily component	Tide and daily surge levels	Tide and seasonal surge levels

2.4 Population exposed

We analyzed the population exposed to flooding by overlaying downscaled inundation depth and population maps. The downscaled inundation depth maps are calculated as the difference between the simulated flood depth and the relative height above the nearest river based on the HydroSheds elevation at 18" resolution (Lehner *et al* 2008) for every unit-catchment, assuming no flood protection. We used the 2010 WorldPop 30" resolution gridded population dataset (Tatem 2017) and resampled it to the resolution of the inundation depth maps using bi-linear interpolation of population density. We assume that if flood depth is larger than zero the total population in that grid cell is exposed. Flood depths are underestimated if surge is ignored in basins where we find a significant positive difference in simulated flood depths in a scenario with compared to a scenario without total surge levels (experiment 1 in Table 2). Finally, we calculated expected annual population exposed by integrating the population exposed at return periods ranging from 1 to 100 years over the flood probability using the trapezoidal rule (e.g. Ward *et al* 2011). Results of the ensemble-mean expected annual population exposed are presented and referred to as population flood exposure.

3 Results and discussion

3.1 Flood drivers

Globally, flood drivers are classified as compound-dominant at 19.7% of the 3433 river mouth locations (Figure 3a), with an average correlation of 0.57 between h_{AM} and skew surge and 0.63 between h_{AM} and discharge at these locations. Flooding is discharge-dominant at 69.2% of locations, with an average correlation of 0.84 between h_{AM} and discharge at these locations, and surge-dominant at 7.8% of locations, with an average correlation of 0.60 between h_{AM} and skew surge at these locations. The remaining 3.3% of locations are classified as insignificant. Generally, compound flood drivers are found around large parts the USA, north-west Europe, the east coast of China at the Yellow Sea, the east coast of Thailand and Malaysia, and around the Australian coastline. These regions are largely similar to those identified with high compound flood potential based on statistical dependence between simulated (Couasnon *et al* 2019) and observed (Ward *et al* 2018) surge and discharge. Notable differences occur along the east coast of the USA and the coast of the Baltic sea, likely due to the different selection criteria for compound events between the studies. For the UK we find a similar spatial pattern of locations with compound drivers compared to locations with a frequent joint occurrence of high skew surges and high river discharge (Hendry *et al* 2019), which are found more often along the west and south coasts relative to the east coast of the UK.

Next, we examined relationships between characteristics of river mouth locations and flood driver classification. Locations with surge- or compound-dominant drivers generally have higher annual maxima skew surge (Figure 4a) and lower long-term average and annual maxima discharge (Figure 4c and 4e) than locations with discharge-dominant drivers. While mean annual maxima skew surge levels are similar between locations with surge- and compound-dominant flood drivers, the inter-annual variability of skew surge (Figure 4b) is generally larger for locations with compound-dominant flood drivers, indicating relatively large skew surge extremes at those locations. The high spatial heterogeneity of flood driver classification is likely due to different catchment characteristics. Generally, compound-dominant flood drivers occur in catchments with smaller area (although the difference is not significant) (Figure 4f), shorter mean drainage length (Figure 4g), and lower mean drainage slope, i.e. flatter topography (Figure 4h). These results are in line with earlier results suggesting that compound events occur more frequently in smaller catchments with a faster response in the UK (Hendry *et al* 2019). In contrast to the results of Hendry *et al* (2019), we find that catchments with compound flood drivers have flatter instead of steeper topography. This could be explained by the selection of compound events: while Hendry *et al* (2019) focus on high surge and high discharge, we also sample events with high surge and moderate discharge. Under these conditions, surge is more likely to propagate up rivers with flat topography.

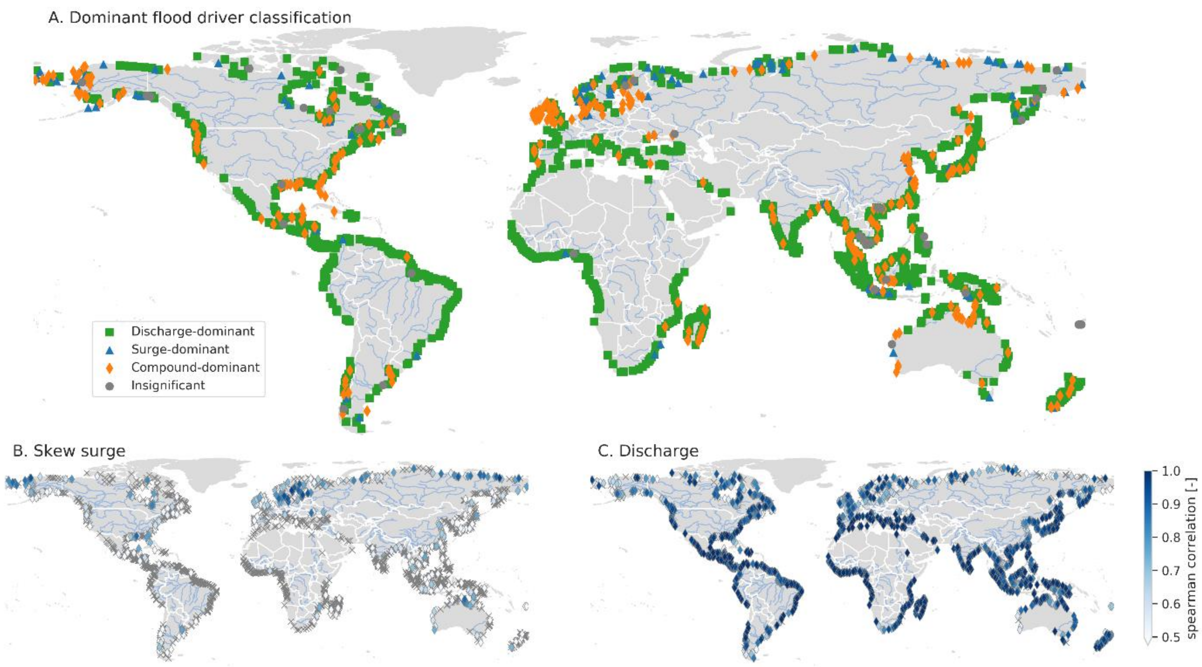

Figure 3: (**a**) Flood driver classification into four classes: surge-dominant (blue), discharge-dominant (green), compound-dominant (orange) or insignificant (grey) based on Spearman rank correlations between (**b**) riverine water level peaks and associated skew surge, and (**c**) riverine water level peaks and associated discharge where crosses indicate insignificant correlation. The largest 2000 out of 3433 rivers in terms of long-term average discharge are shown.

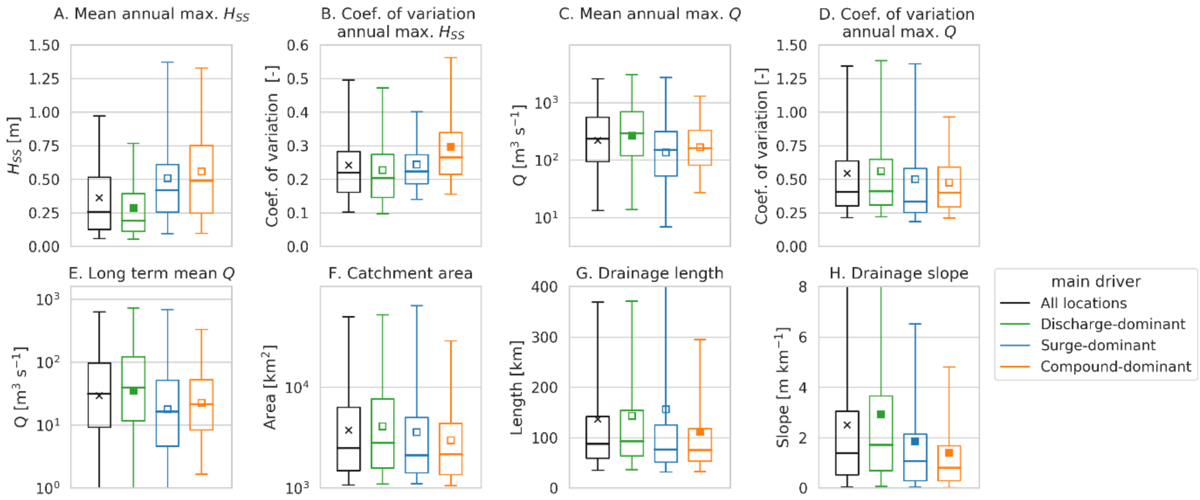

Figure 4: Box-whisker plots showing distributions of river mouth locations characteristics for different classes of flood drivers: discharge-dominant (green), surge-dominant (blue) or compound-dominant (orange); the overall distribution is shown in black. The characteristics are: (**a**) the mean and (**b**) coefficient of variation of annual maxima skew surge (H_{SS}); (**c**) mean and (**d**) coefficient of variation of annual maxima discharge (Q); (**e**) long term mean Q; (**f**) catchment area; (**g**) mean drainage path length; and (**f**) mean drainage path slope. The boxes show the interquartile range (25^{th}-75^{th} percentile), the thick line the median, the whiskers the 5^{th} -95^{th} percentiles, and the markers the mean. The markers are filled if significantly different (p=0.01) from other driver classes based on the Welch's t-test.

3.2 Flood levels

Our results show that 1-in-10 years (T10) flood levels are generally exacerbated due to surge with an overall ensemble-mean difference in riverine water level at the river mouth (Δh) of 11 cm (Fig. Figure 5a). Δh is positive at 64.0% of the 3433 river mouth locations studied, and negative at 12.2%. Moreover, Δh is larger than the 5-95% bootstrap confidence intervals for all ensemble member at 17.3%, while at the 23.9% the ensemble members do not agree on the sign of Δh and are classified as insignificant. Δh is largest at locations with surge-dominant (28 cm) or compound-dominant flood drivers (30 cm), while the Δh is small (3 cm) at locations with discharge-dominant flood drivers. Generally speaking, regions with the largest positive Δh are the coasts of Alaska (US), North-West Europe, the Chinese coast at the Yellow Sea and the coast on the Gulf of Carpentaria (Australia), which are all characterized by large surge extremes. Generally, with increasing return periods, the number of locations with significant Δh decreases due to higher uncertainties, while Δh increases at other locations, see Table 3. To better understand Δh, we divide it into a difference in riverine water level due to a daily (Δh_{daily}) and seasonal component ($\Delta h_{seasonal}$), see Figure 5b-c. The daily component is mainly associated with surge due to short term meteorological variation in wind speed and sea level pressure, while the seasonal component is associated with seasonal gyre circulation (e.g. Yang *et al* 1998, Palma *et al* 2004). Large positive values of Δh are mainly caused by Δh_{daily}, which for T10 is positive at 73.1% of the locations with a mean increase of 14 cm, while negative Δh is mainly caused by $\Delta h_{seasonal}$, which for T10 is negative at 50.3% of the locations with a mean decrease of 3 cm. In some areas, such as most of the South and East coasts of Asia and North coast of Australia, $\Delta h_{seasonal}$ and Δh_{daily} are both positive and combine to a larger positive Δh. Here, positive seasonal effects and the main storm season coincide. For North Australia this is during the Australian-Indonesian monsoon in the local summer months (DJF), which causes large seasonal surge levels (Haigh *et al* 2013a) and is also known to be the season with strong tropical cyclone activity (Haigh *et al* 2013b). This results in strong dependence between surge and precipitation (Wu *et al* 2018). In other areas, such as the coastline of the Hudson Bay (Canada), the Argentinian coast and the South coasts of Australia, a positive Δh_{daily} is alleviated by a negative $\Delta h_{seasonal}$. At the Argentinian coast, negative $\Delta h_{seasonal}$ is caused by offshore wind stress throughout the year (Palma *et al* 2004) while positive Δh_{daily} is caused by large storm surge events, especially around Mar del Plata (Fiore *et al* 2009). Compared to Ikeuchi *et al* (2017) who reported on the effect of total sea level variations on riverine water levels, we find mostly similar areas with large Δh. Notable differences include the Gulf of Carpentaria and North Sea coast where we find larger Δh which can be attributed to relatively large surge levels.

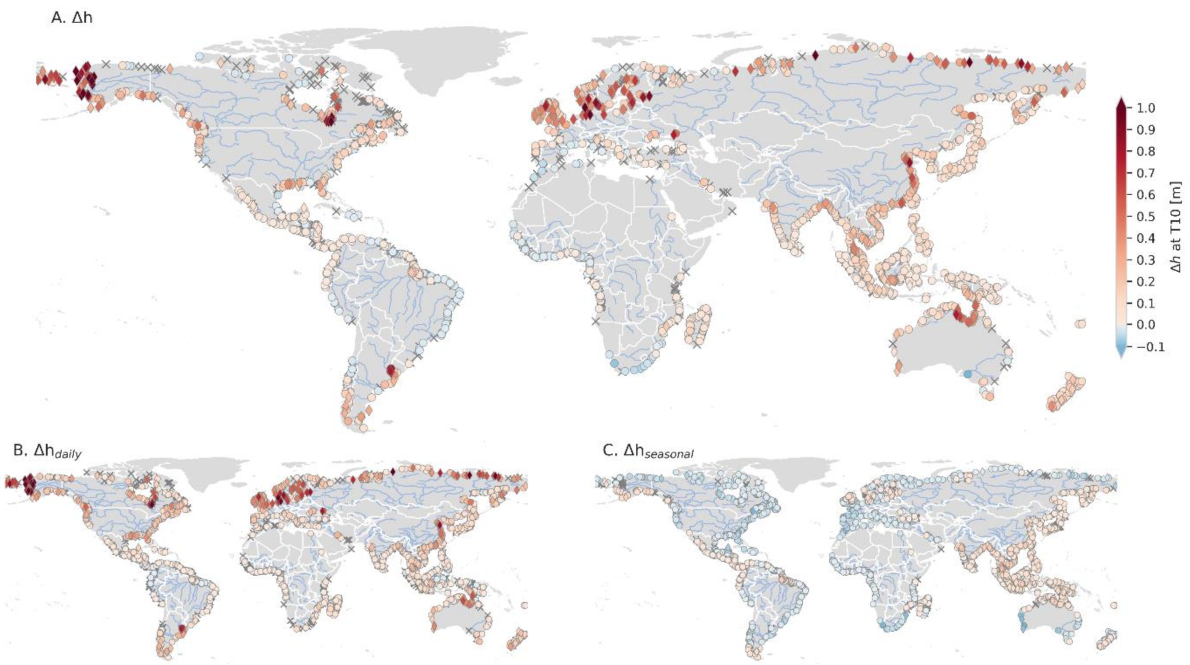

Figure 5: Ensemble-mean difference in 1-in-10 years flood levels at the river mouth due to (**a**) total surge levels; and surge divided into (**b**) a daily and (**c**) a seasonal component. At locations indicated with a diamond, the difference is larger than the 5-95% bootstrap confidence intervals for all ensemble members; at locations indicated with a cross, the sign of difference is not consistent across the

ensemble members. The largest 2000 out of 3433 rivers in terms of long-term average discharge are shown.

Table 3: Percentage of 3433 river mouth locations with an insignificant, positive significant, or negative significant ensemble-mean difference in flood level due to surge, with between brackets the mean difference.

Return period (years)	2	10	50	100
Insignificant	17.9%	23.9%	36.0%	39.6%
Positive significant	66.2% (12 cm)	64.0% (16 cm)	56.1% (22 cm)	53.6% (24 cm)
Negative significant	15.8% (-2 cm)	12.2% (-2 cm)	8.0% (-2 cm)	6.8% (-3 cm)

3.3 Population exposed

If surge is ignored flood depths (and thus flood risk) are significantly underestimated for 30.7 million out of 332.0 million of the total population flood exposure, i.e. 9.3%. In absolute numbers, most people for whom flood depths are underestimated live along the densely populated coasts of east and south Asia. In relative numbers, flood depths are underestimated for a large percentage of the total population flood exposure in small coastal basins with compound- or surge-dominant drivers, but also larger basins along the Hudson Bay coastline (Canada), the Neva (Russia), and the Elbe and Weser (Germany), see Figure 6.

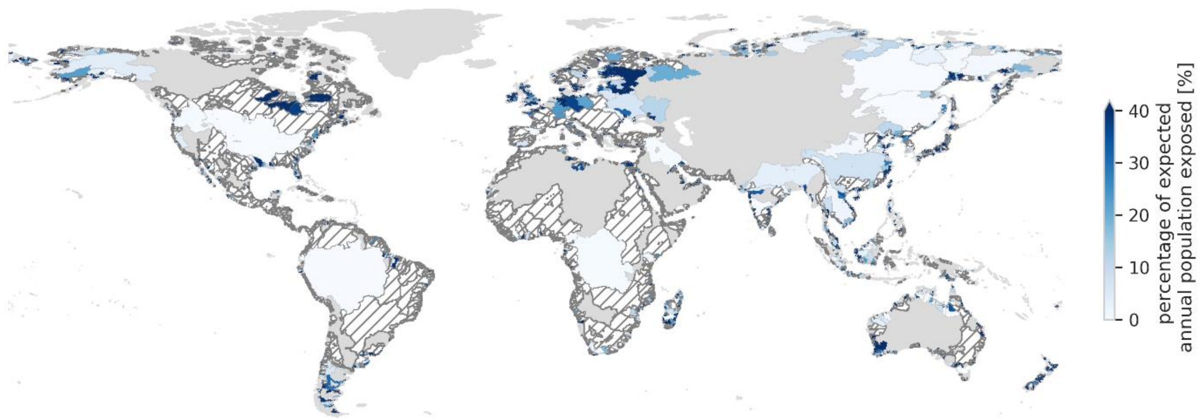

Figure 6: Percentage of ensemble-mean expected annual mean population exposed to riverine flooding for whom flood depths are underestimated if surge is ignored. Hatched basins show insignificant difference in flood depth; grey areas are not simulated (i.e. Greenland and Iceland) or not connected with GTSM (e.g. Irrawaddy). Note that the entire basins are colored while the underestimation of flood depths occurs in the coastal areas of the basin.

3.4 Limitations of the datasets and methods

The magnitude and timing of annual maxima surge and discharge estimates from GTSM and CaMa-Flood are not perfectly resolved, see section 2.2. To account for some of these uncertainties, we used the E2O tier 2 multi-model ensemble. We only used a single surge model as there is less uncertainty in the timing of surge compared to discharge simulations (Couasnon *et al* 2019) and to date there is only one global hydrodynamic surge model with sufficient temporal and spatial resolution for this application.

Some processes that could affect the classification of flood drivers are currently missing in the model framework. GTSM does not account for non-linear surge-tide interactions, or inter-annual variability in mean sea levels due to steric effects or waves, which can be important drivers of coastal flooding at regional scales (e.g. Arns *et al* 2017, Muis *et al* 2018, Vitousek *et al* 2017). CaMa-Flood does not take the operation of reservoirs into account, while these will significantly change the magnitude and timing of discharge peaks (Mateo *et al* 2014, Fleischmann *et al* 2019). Local variations in bathymetry that are not addressed in the CaMa-Flood and/or GTSM models may cause bias in the absolute water levels locally. Near-shore and estuarine areas are still very difficult to resolve accurately in global bathymetry datasets (Weatherall *et al* 2015) and therefore provide large uncertainty for global compound flood risk analysis. The model framework does not account for the influence of discharge on local sea levels as these are derived independently. A two-way coupling between GTSM and CaMa-Flood would be required to assess the complete interactions.

Furthermore, we did not account for uncertainties in the meteorological forcing. While the MSWEP V1.2 precipitation dataset is known to have a good performance compared to many other state-of-the-art global precipitation datasets, it has some caveats, including spurious drizzle and attenuated peaks (Beck *et al* 2017). GTSM is known to underestimate surge in areas with tropical cyclones due to the coarse spatial resolution of ERA-Interim (Muis *et al* 2016, Dullaart *et al* 2019). This might lead to an underestimation of the contribution of surge to riverine flooding in areas with high cyclone activity. Recent updates of meteorological forcing datasets, including MSWEP v2 (Beck *et al* 2018) and ERA5 (the successor to ERA-Interim), could further improve our results.

We estimated flood extent and subsequent flood impact based on downscaled flood depths from CaMa-Flood. We assumed no flood protection to focus on the effect of surge on flood impact as accurate global data on protection standards are sparse (Scussolini *et al* 2016) and simulated flood impacts very sensitive to flood protection (Ward et al 2013). To improve the detail of the flood maps and resolve complex hydrodynamic interactions between different flood drivers in coastal areas, higher resolution and likely a 2D flood model are required. A nested modelling approach (e.g. Hoch *et* *al* 2019) could be a possible avenue to explore in order to improve flood modelling in coastal areas without compromising too much on computationally efficiency.

4 Conclusions and future work

In this study we present the first mapping of the dominant drivers of riverine flooding in deltas globally and assessed the effect of surge on riverine flood hazard and impact. The research highlights the importance of including dynamic sea level boundary conditions in riverine flood risk models. Drivers of riverine flooding are compound-dominant at 19.7% of the locations analyzed, discharge-dominant at 69.2% and surge-dominant at 7.8%. Compared to locations with either surge- or discharge-dominant flood drivers, locations with compound-dominant flood drivers generally have larger surge extremes and are in basins with faster discharge response and/or flat topography. Globally, surge exacerbates T10 flood levels at 64.0% of the locations analyzed, with a mean increase of 11 cm. While this increase is the largest at locations with compound- or surge-dominant flood drivers, surge also affects flood levels at locations with discharge-dominant flood drivers. A small decrease in T10 flood levels is observed at 12.2% of locations analyzed due to negative surge levels associated with dominant seasonal gyre circulations. Finally, we show that if surge is ignored, flood depths are underestimated for 30.7 million out of a total of 332.0 million (9.3%) population flood exposure.

In general, large scale flood risk studies would improve from a more holistic representation of flooding in our models, including direct coastal flooding from storm surges and waves as well as pluvial and fluvial flooding. This may require more detailed 2D hydrodynamic modelling in coastal areas to resolve complex hydrodynamic interactions between these different drivers. While we focused on classifying the drivers of riverine flooding per location, investigating the drivers and meteorological conditions of individual flood events would further enhance our understanding of compound events.

Data Availability

The source code for the simulation, pre- and postprocessing and the analysis is available on GitHub at https://github.com/DirkEilander/compound_hotspots (DOI: 10.5281/zenodo.3665811). The dataset of simulated water levels and discharge at 3433 river mouth locations globally, including several components of nearshore still water levels is available on Zenodo (DOI: 10.5281/zenodo.3665734).

Acknowledgements

The research leading to these results received funding from the Netherlands Organisation for Scientific Research (NWO) in the form of a VIDI grant (grant no. 016.161.324) and the TOUGOU program by MEXT Japan, and JSPS KAKENHI (grant no. JP16J07523).

Competing Financial Interest Statement

The authors declare no competing financial interests.

References

Arns A, Dangendorf S, Jensen J, Talke S, Bender J and Pattiaratchi C 2017 Sea-level rise induced amplification of coastal protection design heights Sci. Rep. 7 40171

Beck H E, Van Dijk A I J M, Levizzani V, Schellekens J, Miralles D G, Martens B and De Roo A P J 2017 MSWEP: 3-hourly 0.25 deg; global gridded precipitation (1979-2015) by merging gauge, satellite, and reanalysis data Hydrol. Earth Syst. Sci. 21 589–615

Beck H E, Wood E F, Pan M, Fisher C K, Miralles D G, van Dijk A I J M, McVicar T R and Adler R F 2018 MSWEP V2 global 3-hourly 0.1° precipitation: methodology and quantitative assessment Bull. Am. Meteorol. Soc. BAMS--D--17--0138.1

Bevacqua E, Maraun D, Vousdoukas M I, Voukouvalas E, Vrac M, Mentaschi L and Widmann M 2019 Higher probability of compound flooding from precipitation and storm surge in Europe under anthropogenic climate change Sci. Adv. 5

Bevacqua E, Maraun D, Hobæk Haff I, Widmann M and Vrac M 2017 Multivariate Statistical Modelling of Compound Events via Pair-Copula Constructions: Analysis of Floods in Ravenna Hydrol. Earth Syst. Sci. Discuss. 1–34

Carrere L, Lyard F, Cancet M, Guillot A and Roblou L 2012 FES2012: A new global tidal model taking advantage of nearly 20 years of altimetry 20 Years of Progress in Radar Altimatry (Venice, Italy) p 6

Cid A, Wahl T, Chambers D P and Muis S 2018 Storm Surge Reconstruction and Return Water Level Estimation in Southeast Asia for the 20th Century J. Geophys. Res. Ocean. 123 437–51

Couasnon A, Eilander D, Muis S, Veldkamp T I E, Haigh I D, Wahl T, Winsemius H C and Ward P J 2019 Measuring compound flood potential from river discharge and storm surge extremes at the global scale and its implications for flood hazard Nat. Hazards Earth Syst. Sci. Discuss. 1–24

Couasnon A, Sebastian A and Morales-Nápoles O 2018 A Copula-Based Bayesian Network for Modeling Compound Flood Hazard from Riverine and Coastal Interactions at the Catchment Scale: An Application to the Houston Ship Channel, Texas Water 10 1190

Dee D P, Uppala S M, Simmons A J, Berrisford P, Poli P, Kobayashi S, Andrae U, Balmaseda M A, Balsamo G, Bauer P, Bechtold P, Beljaars A C M, van de Berg L, Bidlot J, Bormann N, Delsol C, Dragani R, Fuentes M, Geer A J, Haimberger L, Healy S B, Hersbach H, Hólm E V., Isaksen L, Kållberg P, Köhler M, Matricardi M, McNally A P, Monge-Sanz B M, Morcrette J-J, Park B-K, Peubey C, de Rosnay P, Tavolato C, Thépaut J-N and Vitart F 2011 The ERA-Interim reanalysis: configuration and performance of the data assimilation system Q. J. R. Meteorol. Soc. 137 553–97

Dottori F, Szewczyk W, Ciscar J-C, Zhao F, Alfieri L, Hirabayashi Y, Bianchi A, Mongelli I, Frieler K, Betts R A and Feyen L 2018 Increased human and economic losses from river flooding with anthropogenic warming Nat. Clim. Chang. 8

Dullaart J C M, Muis S, Bloemendaal N and Aerts J C J H 2019 Advancing global storm surge modelling using the new ERA5 climate reanalysis Clim. Dyn.

Dutra E, Balsamo G, Calvet J, Munier S, Burke S, Fink G, van Dijk A, Martinez-de la Torre A, van Beek R (L. . P H, de Roo A and Polcher J 2017 Report on the improved Water Resources Reanalysis

Fiore M M E, D'Onofrio E E, Pousa J L, Schnack E J and Bértola G R 2009 Storm surges and coastal impacts at Mar del Plata, Argentina Cont. Shelf Res. 29 1643–9

Fleischmann A, Collischonn W, Paiva R and Tucci C E 2019 Modeling the role of reservoirs versus floodplains on large-scale river hydrodynamics Nat. Hazards 99 1075–104

Haigh I D, MacPherson L R, Mason M S, Wijeratne E M S, Pattiaratchi C B, Crompton R P and George S 2013 Estimating present day extreme water level exceedance probabilities around the coastline of Australia: tropical cyclone-induced storm surges Clim. Dyn. 42 139–57

Haigh I D, Wadey M P, Wahl T, Ozsoy O, Nicholls R J, Brown J M, Horsburgh K and Gouldby B 2016 Spatial and temporal analysis of extreme sea level and storm surge events around the coastline of the UK Sci. Data 3 160107

Haigh I D, Wijeratne E M S S, MacPherson L R, Pattiaratchi C B, Mason M S, Crompton R P and George S 2013 Estimating present day extreme water level exceedance probabilities around the coastline of Australia: tides, extra-tropical storm surges and mean sea level Clim. Dyn. 42 121–38

Hallegatte S S, Green C, Nicholls R J and Corfee-Morlot J 2013 Future flood losses in major coastal cities Nat. Clim. Chang. 3 802–6

Hawkes P J 2008 Joint probability analysis for estimation of extremes J. Hydraul. Res. 46 246–56

Hendry A, Haigh I D, Nicholls R J, Winter H, Neal R, Wahl T, Joly-Laugel A and Darby S E 2019 Assessing the characteristics and drivers of compound flooding events around the UK coast Hydrol. Earth Syst. Sci. 23 3117–39

Hinkel J, Lincke D, Vafeidis A T, Perrette M, Nicholls R J, Tol R S J, Marzeion B, Fettweis X, Ionescu C and Levermann A 2014 Coastal flood damage and adaptation costs under 21st century sea-level rise Proc. Natl. Acad. Sci. 111 3292–7

Hirabayashi Y, Mahendran R, Koirala S, Konoshima L, Yamazaki D, Watanabe S, Kim H and Kanae S 2013 Global flood risk under climate change Nat. Clim. Chang. 3 816–21

Hoch J M, Eilander D, Ikeuchi H, Baart F and Winsemius H C 2019 Evaluating the impact of model complexity on flood wave propagation and inundation extent with a hydrologic-hydrodynamic model coupling framework Nat. Hazards Earth Syst. Sci. 19 1723–35

Hosking J R M and Wallis J R 2005 Regional frequency analysis: an approach based on L-moments (Cambridge University Press)

Ikeuchi H, Hirabayashi Y, Yamazaki D, Muis S, Ward P J, Winsemius H C, Verlaan M and Kanae S 2017 Compound simulation of fluvial floods and storm surges in a global coupled river-coast flood model: Model development and its application to 2007 Cyclone Sidr in Bangladesh J. Adv. Model. Earth Syst. 9 1–32

Jongman B, Ward P J and Aerts J C J H 2012 Global exposure to river and coastal flooding: Long term trends and changes Glob. Environ. Chang. 22 823–35

Kew S F, Selten F M, Lenderink G and Hazeleger W 2013 The simultaneous occurrence of surge and discharge extremes for the Rhine delta Nat. Hazards Earth Syst. Sci. 13 2017–29

Khanal S, Ridder N, Vries H De, Terink W and Hurk B Van Den 2019 Storm Surge and Extreme River Discharge : A Compound Event Analysis Using Ensemble Impact Modeling Front. Earth Sci. 7 1–15

Klerk W J, Winsemius H C, van Verseveld W J, Bakker A M R and Diermanse F L M 2015 The co-incidence of storm surges and extreme discharges within the Rhine–Meuse Delta Environ. Res. Lett. 10 035005

Lamb R, Keef C, Tawn J, Laeger S, Meadowcroft I, Surendran S, Dunning P and Batstone C 2010 A new method to assess the risk of local and widespread flooding on rivers and coasts J. Flood Risk Manag. 3 323–36

Lehner B, Verdin K and Jarvis A 2008 New Global Hydrography Derived From Spaceborne Elevation Data Eos, Trans. Am. Geophys. Union 89 93

Moftakhari H R, Salvadori G, AghaKouchak A, Sanders B F and Matthew R A 2017 Compounding effects of sea level rise and fluvial flooding Proc. Natl. Acad. Sci. 114 9785–90

Muis S, Haigh I D, Guimarães Nobre G, Aerts J C J H and Ward P J 2018 Influence of El Niño-Southern Oscillation on Global Coastal Flooding Earth’s Futur. 6 1311–22

Muis S, Verlaan M, Nicholls R J, Brown S, Hinkel J, Lincke D, Vafeidis A T, Scussolini P, Winsemius H C and Ward P J 2017 A comparison of two global datasets of extreme sea levels and resulting flood exposure Earth’s Futur. 5 379–92

Muis S, Verlaan M, Winsemius H C, Aerts J C J H and Ward P J 2016 A global reanalysis of storm surges and extreme sea levels Nat. Commun. 7 11969

Palma E D, Matano R P and Piola A R 2004 A numerical study of the Southwestern Atlantic Shelf circulation: Barotropic response to tidal and wind forcing J. Geophys. Res. Ocean. 109

Petroliagkis T I 2017 Estimations of statistical dependence as joint return period modulator of compound events. Part I: storm surge and wave height Nat. Hazards Earth Syst. Sci. Discuss. 18 1–46

Pugh D, Woodworth P, Pugh D and Woodworth P 2014 Tidal analysis and prediction Sea-Level Science

Ridder N, de Vries H and Drijfhout S 2018 The role of atmospheric rivers in compound events consisting of heavy precipitation and high storm surges along the Dutch coast Nat. Hazards Earth Syst. Sci. 18 3311–26

Rio M-H, Mulet S and Picot N 2014 Beyond GOCE for the ocean circulation estimate: Synergetic use of altimetry, gravimetry, and in situ data provides new insight into geostrophic and Ekman currents Geophys. Res. Lett. 41 8918–25

Savenije H H G 2005 2 - Tide and estuary shape Salinity and Tides in Alluvial Estuaries ed H H G Savenije (Amsterdam: Elsevier Science Ltd) pp 23–68

Schellekens J, Dutra E, Martínez-De La Torre A, Balsamo G, Van Dijk A I J M, Sperna Weiland F, Minvielle M, Calvet J-C C, Decharme B, Eisner S, Fink G, Flörke M, Peßenteiner S, van Beek R (L. . P H, Polcher J, Beck H E, Orth R, Calton B, Burke S, Dorigo W and Weedon G P 2017 A global water resources ensemble of hydrological models: The eartH2Observe Tier-1 dataset Earth Syst. Sci. Data 9 389–413

Scussolini P, Aerts J C J H, Jongman B, Bouwer L M, Winsemius H C, de Moel H and Ward P J 2016 FLOPROS: an evolving global database of flood protection standards Nat. Hazards Earth Syst. Sci. 16 1049–61

Serafin K A, Ruggiero P, Parker K and Hill D . 2019 What's streamflow got to do with it? A probabilistic simulation of the competing oceanographic and fluvial processes driving along-river extreme water levels Nat. Hazards Earth Syst. Sci.

Stammer D, Ray R D, Andersen O B, Arbic B K, Bosch W, Carrère L, Cheng Y, Chinn D S, Dushaw B D, Egbert G D, Erofeeva S Y, Fok H S, Green J A M, Griffiths S, King M A, Lapin V, Lemoine F G, Luthcke S B, Lyard F, Morison J, Müller M, Padman L, Richman J G, Shriver J F, Shum C K, Taguchi E and Yi Y 2014 Accuracy assessment of global barotropic ocean tide models Rev. Geophys. 52 243–82

Svensson C and Jones D A 2004 Dependence between sea surge, river flow and precipitation in south and west Britain Hydrol. Earth Syst. Sci. 8 973–92

Svensson C and Jones D A 2002 Dependence between extreme sea surge, river flow and precipitation in eastern Britain Int. J. Climatol. 22 1149–68

Tatem A J 2017 WorldPop, open data for spatial demography Sci. Data 4

Vitousek S, Barnard P L, Fletcher C H, Frazer N, Erikson L and Storlazzi C D 2017 Doubling of coastal flooding frequency within decades due to sea-level rise Sci. Rep. 7 1399

Vousdoukas M I, Mentaschi L, Voukouvalas E, Bianchi A, Dottori F and Feyen L 2018 Climatic and socioeconomic controls of future coastal flood risk in Europe Nat. Clim. Chang. 8

Wahl T, Haigh I D, Nicholls R J, Arns A, Dangendorf S, Hinkel J and Slangen A B A 2017 Understanding extreme sea levels for broad-scale coastal impact and adaptation analysis Nat. Commun. 8 1–12

Wahl T, Jain S, Bender J, Meyers S D and Luther M E 2015 Increasing risk of compound flooding from storm surge and rainfall for major US cities Nat. Clim. Chang. 5 1–6

Ward P J, Couasnon A, Eilander D, Haigh I D, Hendry A, Muis S, Veldkamp T I E, Winsemius H C and Wahl T 2018 Dependence between high sea-level and high river discharge increases flood hazard in global deltas and estuaries Environ. Res. Lett. 13 084012

Ward P J, Jongman B, Salamon P, Simpson A, Bates P D, De Groeve T, Muis S, de Perez E C, Rudari R, Trigg M A and Winsemius H C 2015 Usefulness and limitations of global flood risk models Nat. Clim. Chang. 5 712–5

Ward P J, Jongman B, Sperna Weiland F C, Bouwman A, van Beek R (L. . P H, Bierkens M F P P, Ligtvoet W and Winsemius H C 2013 Assessing flood risk at the global scale: Model setup, results, and sensitivity Environ. Res. Lett. 8 44019

Weatherall P, Marks K M, Jakobsson M, Schmitt T, Tani S, Arndt J E, Rovere M, Chayes D, Ferrini V and Wigley R 2015 A new digital bathymetric model of the world's oceans Earth Sp. Sci. 2 331–45

Winsemius H C, Aerts J C J H, van Beek R (L. . P H, Bierkens M F P P, Bouwman A, Jongman B, Kwadijk J C J, Ligtvoet W, Lucas P L, van Vuuren D P and Ward P J 2016 Global drivers of future river flood risk Nat. Clim. Chang. 6 381–5

Wu W, Mcinnes K, O'grady J, Hoeke R, Leonard M and Westra S 2018 Mapping Dependence Between Extreme Rainfall and Storm Surge J. Geophys. Res. Ocean. 1–14

Wu W, Westra S and Leonard M 2017 A basis function approach for exploring the seasonal and spatial features of storm surge events Geophys. Res. Lett. 44 7356–65

Yamazaki D, de Almeida G A M and Bates P D 2013 Improving computational efficiency in global river models by implementing the local inertial flow equation and a vector-based river network map Water Resour. Res. 49 7221–35

Yamazaki D, Kanae S, Kim H and Oki T 2011 A physically based description of floodplain inundation dynamics in a global river routing model Water Resour. Res. 47 1–21

Yang J, Yu L, Koblinsky C J and Adamec D 1998 Dynamics of the seasonal variations in the Indian Ocean from TOPEX/POSEIDON sea surface height and an ocean model Geophys. Res. Lett. 25 1915–8

Zhao F, Veldkamp T I E, Frieler K, Schewe J, Ostberg S, Willner S, Schauberger B, Gosling S N, Schmied H M, Portmann F T, Leng G, Huang M, Liu X, Tang Q, Hanasaki N, Biemans H, Gerten D, Satoh Y, Pokhrel Y, Stacke T, Ciais P, Chang J, Ducharne A, Guimberteau M, Wada Y, Kim H and Yamazaki D 2017 The critical role of the routing scheme in simulating peak river discharge in global hydrological models Environ. Res. Lett. 12 075003

Zheng F, Westra S, Leonard M and Sisson S A 2014 Modeling dependence between extreme rainfall and storm surge to estimate coastal flooding risk Water Resour. Res. 50 2050–71

Zheng F, Westra S and Sisson S A 2013 Quantifying the dependence between extreme rainfall and storm surge in the coastal zone J. Hydrol.

Zscheischler J, Westra S, van den Hurk B J J M, Seneviratne S I, Ward P J, Pitman A, AghaKouchak A, Bresch D N, Leonard M, Wahl T and Zhang X 2018 Future climate risk from compound events Nat. Clim. Chang. 8 469–77